Revision 2

High pressure silica phase transitions: Implications for deep mantle dynamics and silica crystallization in the protocore

Pratik Kr. Das[1*], Chris E. Mohn[1], John P. Brodholt[1,2], Reidar G. Trønnes[1,3]

[1]Centre for Earth Evolution and Dynamics, University of Oslo
[2]Department of Earth Sciences, University College London
[3]Natural History Museum, University of Oslo

Keywords:
Density functional theory, high-pressure silica polymorphs, deep mantle dynamics, silica crystallisation in protocore, modified stishovite, seifertite, pyrite-type silica

Abstract

The subsolidus phase diagram of silica in the 80-220 GPa pressure range was determined by density functional theory (DFT). The transition pressures calculated using the generalized gradient approximation (GGA) in the static limit (at 0 K, without zero point vibrational energy) for the β-stishovite ($CaCl_2$-structure) to seifertite and the seifertite to pyrite-type transitions are 95 and 213 GPa, respectively. These are in good agreement with those calculated using hybrid functionals, giving transition pressures of 96 and 215 GPa. This indicates that previous local density approximation (LDA) results underestimate the transition pressure by 10-15 GPa. Density functional perturbation theory calculations, carried out using GGA within the quasi-harmonic approximations, give Clapeyron slopes of 5.4 and −2.8 MPa/K for the β-stishovite to seifertite and seifertite to pyrite-type transitions, respectively. This suggests that the seifertite-forming transition occurs at 109 GPa (470 km above the core-mantle boundary, CMB) at an ambient mantle geotherm, whereas the pyrite-type transition occurs at 200 GPa (620 km below the CMB) at 4700 K, which is close to the core adiabat. We also calculate the equation of state and show that the stability of seifertite in the lowermost mantle contributes negative buoyancy to recycled oceanic crust, although not as much as in some previous studies. Nevertheless, the increased density of seifertite over β-stishovite may lead to layers with elevated proportions of basaltic material within the large low S-wave velocity provinces. The seifertite to pyrite-type silica transition in the outer core will affect the silica liquidus surface in the system Fe-Si-O and forms a basis for further investigations of silica crystallisation in the protocore.

1. Introduction

High pressure silica minerals are important phases in the lower mantle and potentially in the core. For instance, silica constitutes 15-20 mol% of basaltic material in the lower mantle (Stixrude and Lithgow-Bertelloni 2012) and so its density is important for the buoyancy and the fate of subducted oceanic crust (e.g. Thomson et al. 2019). In particular, silica goes through a number of phase transitions which add to its density. Since silica is not a phase in a pyrolitic mantle, densification of basalt due to silica phase transitions will promote the segregation and enrichment of basaltic material in the lowermost mantle. Its density is also important in evaluating whether recycled oceanic crust can be incorporated into the two large low shear-wave velocity provinces (LLSVPs), as suggested by Hirose et al. (2005), Trønnes (2010), Koelemeijer et al. (2018) and Thomson et al. (2019). The change towards neutral buoyancy of basaltic material relative to peridotite from 750 km depth towards the core-mantle boundary, suggested by Ballmer et al. (2016) and Torsvik et al. (2016), will partly be offset by any densifying phase transition.

High pressure silica phases may also be important in the Earth's core, as it has been suggested that silica may have crystallized from a cooling and Si-saturated protocore during chemical exchange with a basal magma ocean (Hirose et al. 2017; Trønnes et al. 2019). If so, phase transitions such as the transition from seifertite to pyrite-structured silica at core conditions will affect the topology of the silica liquidus surface in the Fe-rich part of the system Fe-Si-O, which governs the potential crystallization of silica in the protocores of terrestrial planets like Venus, Earth, as well as lager "exo-Earths".

Despite the potential importance of silica phase transitions in the deep Earth, there is considerable uncertainty as to where they occur under mantle and core conditions, particularly for the highest pressure transitions. For instance, experimental and theoretical results for the transition from β-stishovite to seifertite at mantle conditions range from about 80 to 140 GPa. A transition at 140 GPa would imply that seifertite does not exist in the mantle, whereas a transition to seifertite at lower pressures may add significant density to subducted oceanic crust.

Similarly, previous determinations of the seifertite to pyrite-structured silica transition also covers a wide pressure range of about 200 to 260 GPa, so better constraints are needed to gain insights into the conditions of possible silica crystallization in the protocores of Earth and other Earth-like planets.

In this paper we seek to clarify the locations and slopes of the β-stishovite to seifertite and seifertite to the pyrite-structured phase transitions, using ab initio computations with the generalised gradient approximation (GGA) combined with the quasi-harmonic approximation (QHA). Because the static limit (0 K) predictions related to the different functionals applied in density functional theory (DFT) vary by about 30 GPa, we have also used the HSE06 hybrid functional. Hybrid functionals include an amount of exact (non-local) Fock exchange, which removes part of the artificial self-interaction error that may hamper conventional GGA. A number of studies (Wilson and Muscat 2002; Heyd and Scuseria 2004; Matsushita et al. 2011; Pierre et al. 2011; Xiao et al. 2013) have demonstrated that hybrid calculations improve the prediction of structural and elastic properties and phase stabilities for a number of minerals where accurate experimental data are available, relative to conventional functionals such as GGA and LDA (local density approximation). For example, Heyd and Scuseria (2004) have shown that HSE06 predicts bond lengths with about 50% smaller errors than GGA and LDA functionals for non-metallic system.

2. Computational methods

We used DFT with projector augmented wave (PAW) potentials as implemented in Vienna ab-initio simulation package (VASP) (Kresse and Furthmüller 1996; Kresse and Joubert 1999). The PAW potentials provided with VASP explicitly treat the [3s3p]-orbitals for silicon and [2s2p]-orbitals for oxygen as valence states. The pseudopotential core radii were 1.005 a.u. and 0.804 a.u. for Si and O, respectively. To describe exchange-correlations, we used GGA as parameterized by Perdew, Burke and Enzerhof (PBE) (Perdew et al. 1996) and the hybrid functional parameterized by Heyd, Scuseria and Ernzerhof (HSE06) (Heyd et al. 2003, 2006). The fraction of exact HF exchange was set to 0.25, and the use of screened Coloumb-like potentials makes HSE06 computationally less expensive than the non-screened PBE0 functional, without loss of any accuracy. Because density functional perturbation theory (DFPT) is not available for HSE06 in VASP5, we report only HSE06 transition pressures in the static limit.

The electronic wave functions were expanded using a set of plane waves with a kinetic energy cutoff (E_{cutoff}) of 700 eV. We used 96-atom simulation cells for all three silica phases: a 2x2x4 supercell for β-stishovite and 2x2x2 supercells for seifertite and pyrite-type silica. Electronic integration over the Brillouin zone was performed using 2x2x3, 2x2x2 and 2x2x2 Monkhorst-Pack k-point grid (Monkhorst and Pack, 1976) for β-stishovite, seifertite and

pyrite-structured silica phases, respectively. The transition pressures calculated using these k-meshes deviate with less than 0.5 GPa compared to the transition pressures calculated using the denser k-meshes of 7x7x8, 5x5x5 and 7x7x7 for β-stishovite, seifertite and pyrite-type silica, respectively. We relaxed the structures (using the conjugate gradient technique) under strict electronic and ionic convergence criteria of 10^{-8} eV and 10^{-7} eV/atom, respectively. Such tight convergence criteria are necessary for the accurate determination of the vibrational spectra, which in turn is essential to calculate the phase diagram accurately.

We used Phonopy (Togo and Tanaka 2015) to calculate thermodynamic properties from the force constants obtained using DFPT. For all the phases, force constants were calculated without constraining their symmetry. Then the thermodynamic properties such as the vibrational contribution to the Helmholtz free energy (F) and entropy (S) were calculated by interpolating, using a 17x17x17 q-point mesh. Such a dense q-mesh is necessary for the accurate calculation of properties at high temperature.

3. Results and discussion

3.1 Phase Transitions

The static limit (0 K) pressures of the investigated phase transitions occur when the enthalpy difference (ΔH) is zero between the phases. Fig. 1 shows ΔH (= $H_{higher\ pressure\ phase} - H_{lower\ pressure\ phase}$) against pressure for the GGA-PBE and hybrid HSE06 functionals. We find that the GGA transition pressures are 95 and 213 GPa for β-stishovite to seifertite and seifertite to pyrite type silica, respectively. These are in excellent agreement with the HSE06 results of 96 and 215 GPa, respectively.

Table 1 summarises the transition pressures (static limit) reported in the literature for the two phase transitions and shows that the different computational studies predict transition pressures that differ by as much as 23 GPa for the β-stishovite to seifertite transition. Our β-stishovite to seifertite static limit transition of 95 GPa is about 11 GPa higher than the corresponding transitions of Teter et al. (1998) and Oganov et al. (2005), obtained with LDA, and Driver et al. (2010) with the WC GGA functional (Wu and Cohen 2006). LDA generally gives 10-16 GPa lower pressure than GGA for such lower mantle phase transitions (Oganov & Ono, 2004; Tsuchiya et al. 2004), and the difference between our results and those of Oganov et al. (2005) are consistent with that. In contrast, our GGA results are about 12 GPa lower than the GGA results of Tsuchiya et al. (2004). However, we note that they used a

different space group for seifertite. As with Oganov et al. (2005), we found the Pbcn structure to be most stable, whereas Tsuchiya et al. (2004) found Pbca. It is not clear why Tsuchiya et al. (2004) found a lower energy for the Pbca phase, but nevertheless, this is the most likely explanation for their higher transition pressure. The GGA static limit transition of 213 GPa for the seifertite to pyrite-structured silica (space group: Pa-3 *[typesetter: please print space gr. Pa bar 3]*) is also, as expected, about 12 GPa higher than the LDA-results of Oganov et al. (2005).

The Clapeyron slopes for the two phase transitions were obtained using DFPT within the QHA as described in section 2. Fig. 2 shows ΔG as a function of temperature along a range of pressure contours. With increasing pressure, the transition temperatures for the β-stishovite to seifertite and the seifertite to pyrite-type transitions increases and decreases, respectively, implying positive and negative Clapeyron slopes. The negative Clapeyron slope for the transition to the pyrite-structure is due to the increase in entropy, which can be explained by the change in polyhedral connectivity of the SiO_6 octahedra following the phase transition. Whereas the SiO_6 octahedra share both corners and edges in seifertite, they only share corners in the more symmetrical pyrite-structured phase. This is confirmed from the phonon density of states in Fig. 3, which shows that the pyrite-type phase has a higher population of vibrational density of states at the lower energy range, indicating a high entropy contribution to the free energy. A simple and qualitative analysis of Clapeyron slopes for such isochemical phase transitions, characterized by negative volume changes, may be done by comparing the phase entropies at a point on the phase boundaries. The entropies calculated for coexisting β-stishovite and seifertite at 2400 K and 109 GPa, on the ambient mantle geotherm of Stixrude et al. (2009), are 4624 and 4603 J (mol K)$^{-1}$, respectively, yielding a negative ΔS and a positive dp/dT slope. The entropies of seifertite and pyrite-type silica at 4650 K and 201 GPa, on an estimated outer core adiabat (e.g. Olson et al. 2015), are 5866 and 5888 J (mol K)$^{-1}$, respectively, resulting in positive ΔS and negative dp/dT.

The phase relations from our DFT study, as well as from other theoretical and experimental investigations on the two silica phase transitions, are listed in Table 1. Fig. 4 shows the stability fields of the three silica polymorphs in the 80-270 GPa range. The previous experimental and theoretical investigations (Akins and Ahrens 2002; Murakami et al. 2003; Tsuchiya et al. 2004; Kuwayama et al. 2005; Oganov et al. 2005; Driver et al. 2010; Grocholski et al. 2013) cover a range of almost 40 GPa for the β-stishovite to seifertite and more than 60 GPa for the seifertite to pyrite-type silica transitions. Our phase boundaries are

inside these ranges and in good agreement with the LDA results of Oganov et al. (2005), taking into account that the LDA functional produces 10-16 GPa lower static limit pressures than GGA. Our calculated slopes of about +5.4 and −2.8 MPa/K for the β-stishovite to seifertite and seifertite to pyrite-type silica transitions, respectively, are also similar to the corresponding transition slopes of Oganov et al. (2005) (Table 1).

The β-stishovite to seifertite boundary slope of 5.4 MPa/K is also very similar to (slightly lower than) that of Tsuchiya et al. (2004), even if they used a different space group for seifertite. Driver et al. (2010) report a higher dp/dT slope, which is closer to the slopes suggested by the experimental studies of Murakami et al. (2003) and Grocholski et al. (2013). The dp/dT slope proposed in the phase diagram of Akins et al. (2002) has the lowest value of 3.9 MPa/K. A common feature for all the experimental studies, however, is that the slopes are ill-constrained, and Murakami et al. (2003) drew a linear phase boundary from their experimental determination of the phase transition at 2300 K and 120 GPa to the static limit (0 K) pressure of 98 GPa from the Karki et al. (1997) LDA-based investigation. Although the phase boundary derived by Grocholski et al. (2013) is broadly consistent with their experiments on a pure SiO_2 composition, it is mostly constrained by experiments on a composition with 90 and 10 mol% SiO_2 and Al_2O_3, respectively.

The extreme pressures involved in the experimental determination of the seifertite to pyrite-structured silica transition by Kuwayama et al. (2005), made it challenging to constrain a Clapeyron slope. The four experiments close to the recorded transition indicate a flat dp/dT slope. The low temperatures of 1400-2000 K, however, might have caused slow kinetics, which has also been observed for the β-stishovite to seifertite transition (Murakami et al. 2003), resulting in excessively high pressure before the transition could be seen in the XRD patterns. Because LDA determinations of high pressure phase transitions generally give pressures that are 10-16 GPa lower than the equivalent GGA results (Oganov and Ono 2004; Tsuchiya et al. 2004), the agreement in terms of pT-locations and Clapeyron slopes for the β-stishovite to seifertite and seifertite to pyrite-structured silica transitions derived by Oganov et al. (2005) and this study is reassuring.

Our results indicate that the seifertite-forming reaction in basaltic materials may occur as much as 477 km above the core-mantle boundary (CMB) along the ambient mantle geotherm of Stixrude et al. (2009), using the pressure-depth relation of the PREM model (Dziewonski and Anderson 1981). Although the Stixrude et al. (2009) geotherm is drawn to a CMB-temperature of 4100 K, we have adjusted the geotherms to a lower CMB temperature

of 4000 K, in accordance with most studies (e.g. Trønnes et al. 2019). Based on a recent experimental investigation of iron melting, Sinmyo et al. (2019) suggest an even lower CMB temperature. Seifertite is stabilised to relatively shallow levels even in a hot mantle, and at 500 K above the ambient geotherm, the seifertite-forming transition would occur about 427 km above the CMB, using our GGA transition. At a cold slab geotherm about 800 K below ambient conditions at 60-70 GPa (Nishi et al. 2014) and 740 K below ambient conditions at 100 GPa, the seiferite transition would occur about 550 km above the CMB. We have not considered here the effect of Al on the phase transitions. Although a strong partitioning of Al into seifertite as indicated by Hirose et al. (2005) would lower the transition pressure further (Andrault et al. 2014), a recent study of Tateno et al. (2018) indicates that Al partitions weakly into β-stishovite relative to seifertite. In any case, our evidence points to a wide stability field of seifertite in basaltic lithologies in the lowermost mantle.

3.2 Volumes and equation of state

Fig. 5 shows the equations of state for β-stishovite and seifertite, obtained from GGA and HSE06 functionals, compared to available experimental results (Murakami et al. 2003; Grocholski et al. 2013; Fischer et al. 2018). We find that GGA at 300 K predicts about 2% larger volumes than the experimental results at any given pressure. This is normal behaviour for the GGA functional, which often predicts larger volumes than experiments by a few percent. On the other hand, the HSE06 volume predictions are only about 0.5% above, whereas the LDA results of Yang and Wu (2014) for β-stishovite coincides with, the experimental data. At any given volume, the GGA-based pV-curves for β-stishovite and seifertite are about 15 and 19 GPa above the experimentally determined data, respectively. These deviations are somewhat larger than that of bridgmanite (Zhang et al. 2013), and they reflect the larger bulk moduli of the silica minerals, and especially of seifertite (Table 2). The functional forms of the equations of state based on GGA and the experiments are essentially identical. Van de Walle and Ceder (1999) proposed a linear correction to volume-dependent internal energy, which is equivalent to a constant shift in the pressure. This type of correction was used by several authors, e.g., Oganov et al. (2001), Wentzcovitch et al. (2004), Stixrude and Karki (2005). In order to derive optimal density estimates, we therefore apply pressure corrections of −15 and −19 GPa for β-stishovite and seifertite, respectively, to the GGA results. After this simple adjustment, the corrected GGA pV-curves are in excellent agreement with the experimental results over the full range of pressure.

The LDA calculations of Oganov et al. (2005) predicted zero pressure volumes for β-stishovite and seifertite of 23.6 and 22.8 $Å^3/SiO_2$-unit, respectively, compared to 24.2 and 23.6 $Å^3/SiO_2$-unit from our GGA calculations. The HSE06 calculations predicted zero pressure volumes of 22.7 and 22.2 $Å^3/SiO_2$-unit for β-stishovite and seifertite, respectively. To calculate HSE06-based equations of state for a temperature of 300 K in Fig. 5, we added the GGA-derived volume increase in the 0-300 K range to the volume predicted by HSE06 at 0 K. The HSE06-based equations of state agree well with the experimentally derived values for both SiO_2 phases.

Our static limit calculations, using a third order Birch-Murnaghan equation of state, of bulk moduli for β-stishovite and seifertite gave 283 and 312 GPa, respectively, using the GGA functional and 315 and 320 GPa, respectively, with HSE06. These are in good agreement with previous experimental and theoretical studies (Dubrovinsky et al. 2001; Andrault et al. 2003; Murakami et al. 2003; Oganov et al. 2005; Driver et al. 2010; Grocholski et al. 2013).

We have also calculated the density of all three phases at high pressure and temperature. The results for β-stishovite agree very well with those measured by Fisher et al. (2018). The pVT volumes were fit to a Mie-Gruneisen-Debye type equation of state, using the BurnMan tool kit (Cottaar et al., 2014), and the EoS parameters are given in Table 2.

4. Implications

Our wide stability field for seifertite would increase the buoyancy contrast of subducted oceanic crust in the lower mantle, increasing the ability for the recycled crust to segregate into LLSVPs and maintain their stability. The effectiveness of this depends on the density contrast between β-stishovite and seifertite. These densities along the mantle adiabat of (Brown and Shankland 1981) are shown in Fig. 6. We also compare with the HeFESTo-based densities for stishovite (β-stishovite is not differentiated from stishovite in that thermodynamic database) and seifertite of Stixrude and Lithgow-Bertelloni (2011), as well as the experimentally obtained density for β-stishovite of Fischer et al. (2018). Our β-stishovite density curve is slighty above that of Fischer et al. (2018), but agrees to within 0.25%. In contrast, our seifertite density is about 2% lower than that from the HeFESTo database, which does not provide data for β-stishovite (only for stishovite). We also find a smaller

density jump at the phase transition at 109 GPa and 2400 K of about 0.7 %, whereas HeFESTo predicts a larger jump of about 1.5 % from stishovite to seifertite. The small density jump at the transition means that the β-stishovite to seifertite transition is unlikely to produce a significant density increase in subducting slabs, containing 6-7 vol% basaltic crust. Even with as much as 18 mol% silica phases in pure basaltic material, the transition may only add an increment of about 0.1% to the density of potential LLSVP-material containing efficiently segregated (100%) oceanic crust.

Unequivocal observations of seismic discontinuities caused by the seifertite-forming reaction in the mantle are not available, although Ohta et al. (2008) tentatively connect a seismic discontinuity about 470 km above the CMB inside the Pacific LLSVP, 7-15º SSE of Hawaii, to the combination of the seifertite- and post-bridgmanite-forming transitions in basaltic material. This depth is in reasonable agreement with our predicted phase transition.

At greater pressures, the seifertite to pyrite-structured silica phase transition will affect the shape of the silica liquidus for melt compositions in the Fe-rich part of the Fe-Si-O system. Further constraints on the dT/dp-slopes of silica liquidi for relevant core compositions and on outer core adiabats will determine if silica would have crystallised in the uppermost or in the deeper regions of the core (Hirose et al. 2017; Trønnes et al. 2019). This information is required in order to judge whether a stagnant E'-layer, depleted in Si and enriched in O, could have been formed by silica crystallisation (Brodholt and Badro 2017; Trønnes et al. 2019).

Acknowledgements

The Centre for Earth Evolution and Dynamics is funded by CoE-grant 223272 from the Research Council of Norway, and the computational resources are provided by the Norwegian infrastructure for high-performance computing via NOTUR grants NN9329K and NN2916K. Two anonymous reviewers provided useful corrections and suggestions for improvements.

References

Akins, J.A., and Ahrens, T.J. (2002) Dynamic compression of SiO_2: A new interpretation . Geophysical Research Letters, 29, 31-1-31–4.

Andrault, D., Angel, R.J., Mosenfelder, J.L., and Le Bihan, T. (2003) Equation of state of stishovite to lower mantle pressures. American Mineralogist, 88, 301–307.

Andrault, D., Trønnes, R.G., Zonopkova, Z., Morgenroth, W., Liermann, H.P., Morard, G.,

and Mezouar, M. (2013) Phase transition in Al-bearing SiO_2 and P-V-T equation of state of seifertite at lowermost mantle conditions. American Mineralogist, 99, 2035–2042.
Ballmer, M.D., Schumacher, L., Lekic, V., Thomas, C., and Ito, G. (2016) Compositional layering within the large low shear-wave velocity provinces in the lower mantle. Geochemistry, Geophysics, Geosystems, 17, 5056–5077.
Brodholt, J., and Badro, J. (2017) Composition of the low seismic velocity E′ layer at the top of Earth's core. Geophysical Research Letters, 44, 8303–8310.
Brown, J.M., and Shankland, T.J. (1981) Thermodynamic parameters in the Earth as determined from seismic profiles. Geophysical Journal of the Royal Astronomical Society, 66, 579–596.
Cottaar, S., Heister, T., Rose, I., and Unterborn, C. (2014) BurnMan: a lower mantle mineral physics toolkit. Geochemistry, Geophysics, Geosystems 15, 1164-1179.
Driver, K.P., Cohen, R.E., Wu, Z., Militzer, B., Rios, P.L., Towler, M.D., Needs, R.J., and Wilkins, J.W. (2010) Quantum Monte Carlo computations of phase stability, equations of state, and elasticity of high-pressure silica. Proceedings of the National Academy of Sciences, 107, 9519–9524.
Dubrovinsky, L.S., Dubrovinskaia, N.A., Saxena, S.K., Tutti, F., Rekhi, S., Bihan, T. Le, Shen, G., and Hu, J. (2001) Pressure-induced transformations of cristobalite. Chemical Physics Letters, 333, 264–270.
Dziewonski, A.M., and Anderson, D.L. (1981) Preliminary reference Earth model. Physics of the Earth and Planetary Interiors, 25, 297–356.
Fischer, R.A., Campbell, A.J., Chidester, B.A., Reaman, D.M., Thompson, E.C., Pigott, J.S., Prakapenka, V.B., and Smith, J.S. (2018) Equations of state and phase boundary for stishovite and $CaCl_2$ -type SiO_2. American Mineralogist, 103, 792–802.
Grocholski, B., Shim, S.H., and Prakapenka, V.B. (2013) Stability, metastability, and elastic properties of a dense silica polymorph, seifertite. Journal of Geophysical Research E: Planets, 118, 4745–4757.
Heyd, J., and Scuseria, G.E. (2004) Efficient hybrid density functional calculations in solids: Assessment of the Heyd-Scuseria-Ernzerhof screened Coulomb hybrid functional. Journal of Chemical Physics, 121, 1187–1192.
Heyd, J., Scuseria, G.E., and Ernzerhof, M. (2003) Hybrid functionals based on a screened Coulomb potential. Journal of Chemical Physics, 118, 8207–8215.
Heyd, J., Scuseria, G.E., and Ernzerhof, M. (2006) Erratum: Hybrid functionals based on a screened Coulomb potential (Journal of Chemical Physics (2003) 118 (8207)). Journal of Chemical Physics, 124, 219906–1.
Hirose, K., Takafuji, N., Sata, N., and Ohishi, Y. (2005) Phase transition and density of subducted MORB crust in the lower mantle. Earth and Planetary Science Letters, 237, 239–251.
Hirose, K., Morard, G., Sinmyo, R., Umemoto, K., Hernlund, J., Helffrich, G., and Labrosse, S. (2017) Crystallization of silicon dioxide and compositional evolution of the Earth's core. Nature, 543, 99.
Karki, B.B., Warren, M.C., Stixrude, L., Ackland, G.J., and Crain, J. (1997) Ab initio studies of high-pressure structural transformations in silica. Physical Review B, 55, 3465–3471.
Koelemeijer, P., Schuberth, B.S.A., Davies, D.R., Deuss, A., and Ritsema, J. (2018) Constraints on the presence of post-perovskite in Earth's lowermost mantle from tomographic-geodynamic model comparisons. Earth and Planetary Science Letters, 494, 226–238.
Kresse, G., and Furthmüller, J. (1996) Efficient iterative schemes for ab initio total-energy calculations using a plane-wave basis set. Physical Review B, 54, 11169–11186.
Kresse, G., and Joubert, D. (1999) From ultrasoft pseudopotentials to the projector

augmented-wave method. Phys. Rev. B, 59, 1758–1775.
Kuwayama, Y., Hirose, K., Sata, N., and Ohishi, Y. (2005) The Pyrite-Type High-Pressure Form of Silica. Science, 309, 923–925.
Matsushita, Y.I., Nakamura, K., and Oshiyama, A. (2011) Comparative study of hybrid functionals applied to structural and electronic properties of semiconductors and insulators. Physical Review B - Condensed Matter and Materials Physics, 84, 1–13.
Murakami, M., Hirose, K., Ono, S., and Ohishi, Y. (2003) Stability of $CaCl_2$-type and α-PbO_2-type SiO_2 at high pressure and temperature determined by in-situ X-ray measurements. Geophysical Research Letters, 30, 11-1-11–4.
Nishi, M., Irifune, T., Tsuchiya, J., Tange, Y., Nishihara, Y., Fujino, K., and Higo, Y. (2014) Stability of hydrous silicate at high pressures and water transport to the deep lower mantle. Nature Geoscience, 7, 224–227.
Oganov, A.R., Brodholt, J.P., Price, G.D., 2001a. Ab initio elasticity and thermal equa- tion of state of MgSiO3 perovskite. Earth Planet. Sci. Lett. 184, 555–560.
Oganov, A.R., and Ono, S. (2004) Theoretical and experimental evidence for a post-perovskite phase of $MgSiO_3$ in Earth's D″ layer. Nature, 430, 445–448.
Oganov, A.R., Gillan, M.J., and Price, G.D. (2005) Structural stability of silica at high pressures and temperatures. Physical Review B, 71, 1–8.
Ohta, K., Hirose, K., Lay, T., Sata, N., and Ohishi, Y. (2008) Phase transitions in pyrolite and MORB at lowermost mantle conditions: Implications for a MORB-rich pile above the core-mantle boundary. Earth and Planetary Science Letters, 267, 107–117.
Olson, P., Deguen, R., Rudolph, M.L., Zhong, S., 2015. Core evolution driven by mantle global circulation. Physics of Earth and Planetary Interiors 243, 44–55.
Pack, J.D., and Monkhorst, H.J. (1977) 'Special points for Brillouin-zone integrations'-a reply. Physical Review B, 16, 1748–1749.
Perdew, J.P., Burke, K., and Ernzerhof, M. (1996) Generalized Gradient Approximation Made Simple. Physical Review Letters, 77, 3865–3868.
Pierre, M.D. La, Orlando, R., Maschio, L., Doll, K., Ugliengo, P., and Dovesi, R. (2011) Performance of Six Functionals (LDA, PBE, PBESOL, B3LYP, PBE0, and WC1LYP) in the Simulation of Vibrational and Dielectric Properties of Crystalline Compounds. The Case of Forsterite Mg_2SiO_4. Journal of Computational Chemistry, 32, 1775–1784.
Sinmyo, R., Hirose, K., Ohishi, Y. (2019) Melting curve of iron to 290 GPa determined in a resistance-heated diamond-anvil cell. Earth and Planetary Science Letters, 510, 45-52.
Stixrude, L., Karki, B. (2005) Structure and freezing of MgSiO3 liquid in Earth's lower mantle. Science 310, 297–299.
Stixrude, L., de Koker, N., Sun, N., Mookherjee, M., and Karki, B.B. (2009) Thermodynamics of silicate liquids in the deep Earth. Earth and Planetary Science Letters, 278, 226–232.
Stixrude, L., and Lithgow-Bertelloni, C. (2011) Thermodynamics of mantle minerals - II. Phase equilibria. Geophysical Journal International, 184, 1180–1213.
Stixrude, L., and Lithgow-Bertelloni, C. (2012) Geophysics of Chemical Heterogeneity in the Mantle. Annual Review of Earth and Planetary Sciences, 40, 569–595.
Tateno, S., Hirose, K., Sakata, S., Yonemitsu, K., Ozawa, H., Hirata, T., Hirao, N., and Ohishi, Y. (2018) Melting Phase Relations and Element Partitioning in MORB to Lowermost Mantle Conditions. Journal of Geophysical Research: Solid Earth, 123, 5515–5531.
Teter, D.M., Hemley, R.J., Kresse, G., and Hafner, J. (1998) High pressure polymorphism in silica. Physical Review Letters, 80, 2145–2148.
Thomson, A.R., Crichton, W.A., Brodholt, J.P., Wood, I.G., Siersch, N.C., Muir, J., Dobson,

D.P., and Hunt, S.A. (2019) Calcium silicate perovskite's seismic velocities can explain LLVPs in Earth's lower mantle. Nature, In press.
Togo, A., and Tanaka, I. (2015) First principles phonon calculations in materials science. Scripta Materialia, 108, 1–5.
Torsvik, T.H., Steinberger, B., Ashwal, L.D., Doubrovine, P. V., and Trønnes, R.G. (2016) Earth evolution and dynamics—a tribute to Kevin Burke. Canadian Journal of Earth Sciences, 53, 1073–1087.
Trønnes, R.G. (2010) Structure, mineralogy and dynamics of the lowermost mantle. Mineralogy and Petrology, 99, 243–261.
Trønnes, R.G., Baron, M.A., Eigenmann, K.R., Guren, M.G., Heyn, B.H., Løken, A., and Mohn, C.E. (2019) Core formation, mantle differentiation and core-mantle interaction within Earth and the terrestrial planets. Tectonophysics, 760, 165–198.
Tsuchiya, T., Caracas, R., and Tsuchiya, J. (2004) First principles determination of the phase boundaries of high-pressure polymorphs of silica. Geophysical Research Letters, 31, 1–4.
Van de Walle, A., Ceder, G., (1999) Correcting overbinding in local-density- approximation calculations. Phys. Rev. B 59, 14992–15001.
Wentzcovitch, R.M., Karki, B.B., Cococcioni, M., de Gironcoli, S.(2004) Thermoelastic properties of $MgSiO_3$-perovskite: Insights on the nature of the Earth's lower mantle. Phys. Rev. Lett. 92, 018501.
Wilson, N., and Muscat, J. (2002) The calculation of structural, elastic and phase stability properties of minerals using first principles techniques: A comparison of HF, DFT and hybrid functional treatments of exchange and correlation. Molecular Simulation, 28, 903–915.
Wu, Z., and Cohen, R.E. (2006) More accurate generalized gradient approximation for solids. Physical Review B - Condensed Matter and Materials Physics, 73, 235116-1–6.
Xiao, B., Sun, J., Ruzsinszky, A., Feng, J., Haunschild, R., Scuseria, G.E., and Perdew, J.P. (2013) Testing density functionals for structural phase transitions of solids under pressure: Si, SiO_2, and Zr. Physical Review B - Condensed Matter and Materials Physics, 88, 184103(1–17).
Yang, R. and Wu, Z. (2014) Elastic properties of stishovite and the $CaCl_2$-type silica at the mantle temperature and pressure: An ab initio investigation. Earth and Planetary Science Letters, 404, pp.14-21.
Zhang, Z., Stixrude, L., and Brodholt, J. (2013) Elastic properties of $MgSiO_3$-perovskite under lower mantle conditions and the composition of the deep Earth. Earth and Planetary Science Letters, 379, 1–12.

Table Captions

TABLE 1: Phase transition pressures (GPa) and Clapeyron slope (MPa/K).
TABLE 2: Equation of state parameters for all three silica phases from this study (Mie-Gruneisen EoS). The equation of state parameters were obtained by fitting to the pressure-corrected GGA results, as discussed in the text.

Figure Captions

FIGURE 1. Enthalpy change upon the phase transition from (a) β-stishovite to seifertite and (b) seifertite to pyrite-type silica as a function of pressure in the static limit, determined using the GGA-PBE (red) and HSE06 (blue) functionals.

FIGURE 2. Gibbs free energy change upon the phase transition from β-stishovite to seifertite (upper panel) and seifertite to pyrite-type silica (lower) as a function of pressure (contour values in GPa) and temperature, calculated with the GGA functional. The transition pressure increases (positive dp/dT slope) and decreases (negative dp/dT slope) with increasing temperature for the β-stishovite to seifertite and seifertite to pyrite-type phase boundaries, respectively.

FIGURE 3. Calculated total phonon density of states of three SiO_2 phases from *ab-initio* lattice dynamics. The phDOS is scaled to 3N (N = no. of atoms).

FIGURE 4. Phase boundaries for the β-stishovite to seifertite and seifertite to pyrite-structured silica. The present results are displayed together with previous results (dashed and solid lines represent experimental and theoretical results, respectively). Static transition pressures are without zero point energy correction. The seifertite-forming transition of Stixrude and Lithgow-Bertelloni (2011) is fixed to the Murakami et al. (2003) transition. Experiments on compositions with 10 mol% Al_2O_3 form the lower bracket for β-stishovite stability in the Grocholski et al. (2013) study.Within the adiabatic range, the geotherm of Stixrude et al. is only about 5 K above the Brown and Shankland (1981) geotherm at pressures above 80 GPa.

FIGURE 5. Equations of state for β-stishovite and seifertite. The HSE06-based EoS (adjusted to 300 K by adding the GGA-derived volume increase from 0 to 300 K) is similar to the 300 K experimental data of Grocholski et al. (2013), Murakami et al. (2003) and Fischer et al. (2018). The LDA results of Yang and Wu (2014) coincides with the experimental data and the present GGA-based pV-curve has the same functional form as the experimental EoS. To obtain optimal density estimates in Fig. 6, the GGA-curves were adjusted downwards by 15 and 19 GPa for β-stishovite and seifertite, respectively.
Comment to the phase transitions in Fig. 4: Because the GGA-volume of each phase is about 2% larger that the experimentally based volumes in Fig. 5, this difference will be *roughly* cancelled out in $\Delta V = V_{seif} - V_{\beta\text{-stish}}$ and the Clapeyron relation, $dp/dT = \Delta S/\Delta V$. Because the static limit GGA and HSE06 pressures for the β-stishovite to seifertite and seifertite to pyrite-type phase transitions differ by only 1.0 and 0.8 %, respectively (Fig. 1), we have not employed any volume or pressure correction to the phase transitions in Fig. 4.

Figure 6. Density of silica phases calculated by the BurnMan code (Cottaar et al., 2014) along the default adiabat of Brown and Shankland (1981), extended to 136 GPa and about 2450 K. Our predicted density for seifertite is 1.5 % lower than the HeFESTo-value of Stixrude and Lithgow-Bertelloni (2011). The density curves are truncated at the seifertite-forming boundary (at 109 GPa and 2400 K). Note that the Stixrude and Lithgow-Bertelloni (2011) density curve below the seifertite stability range is for stishovite, rather than for β-stishovite.

TABLE 1: Phase transition pressures (GPa) and Clapeyron slope (MPa/K).

	β-stishovite → seifertite			**seifertite → Pyrite**		
Theoretical work:	**0 K**	**2500 K**	dp/dT	**0 K**	**2500 K**	dp/dT
This work (GGA)	95	109.2	5.4	213	208.4	-2.8
This work (HSE06)	96	-		215	-	
Teter et al., 1998 (LDA)	85					
Tsuchiya et al., 2004 (GGA)	106.3	120.6	5.7			
Tsuchiya et al., 2004 (LDA)	96.3					
Oganov et al., 2005 (LDA)	84	98.4	6.6	201.5	198.5	-2.9
Driver et al., 2010 (GGA,WC)	83.5	100.7	7.2			
Experimental work:						
Akins et al., 2002 (Dyn. Compres.)		91.4	3.9			
Murakami et al., 2003 (LHDAC)		122	9.5			
Kuwayama et al., 2005 (XRD)					262.5	~ 0*
Grocholski et al., 2013 (DAC)		129.4	6.9			

*tentative slope by Kuwayama et al. (2005)

TABLE 2: Equation of state parameters for all three silica phases from this study (Mie-Gruneisen EoS). The equation of state parameters were obtained by fitting to the pressure-corrected GGA results, as discussed in the text.

	V_0 (cm^3/mol)	K_0 (GPa)	K_0'	γ_0	q_0	θ_T (K)
β-stishovite	14.19 ± 0.01	278 ± 3	4.30 ± 0.05	1.25 ± 0.01	1.18 ± 0.07	1150 ± 10
Seifertite	13.578 ± 0.001	365.7 ± 0.4	3.822 ± 0.003	1.242 ± 0.002	1.23 ± 0.01	1269 ± 6
Pyrite	12.97 ± 0.02	393 ± 5	3.83 ± 0.03	1.448 ± 0.008	1.66 ± 0.04	1219 ± 1

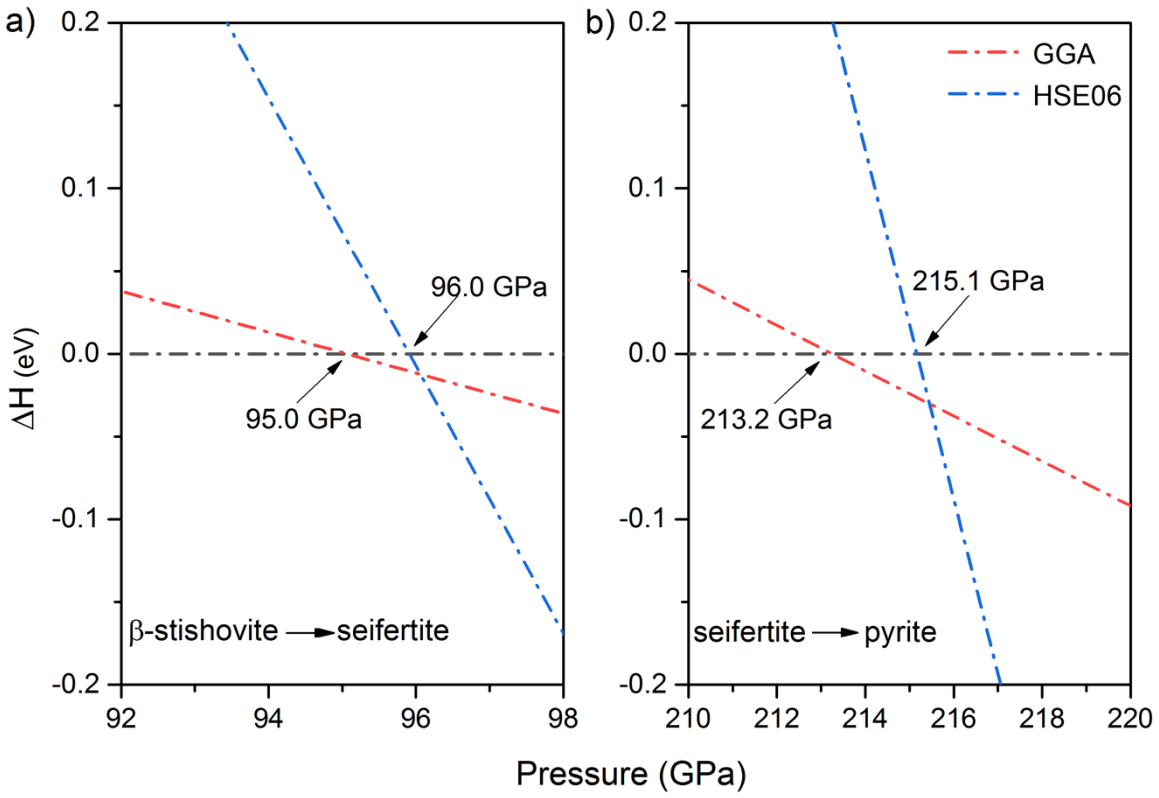

FIGURE 1. Enthalpy change upon the phase transition from (a) β-stishovite to seifertite and (b) seifertite to pyrite-type silica as a function of pressure in the static limit, determined using the GGA-PBE (red) and HSE06 (blue) functionals.

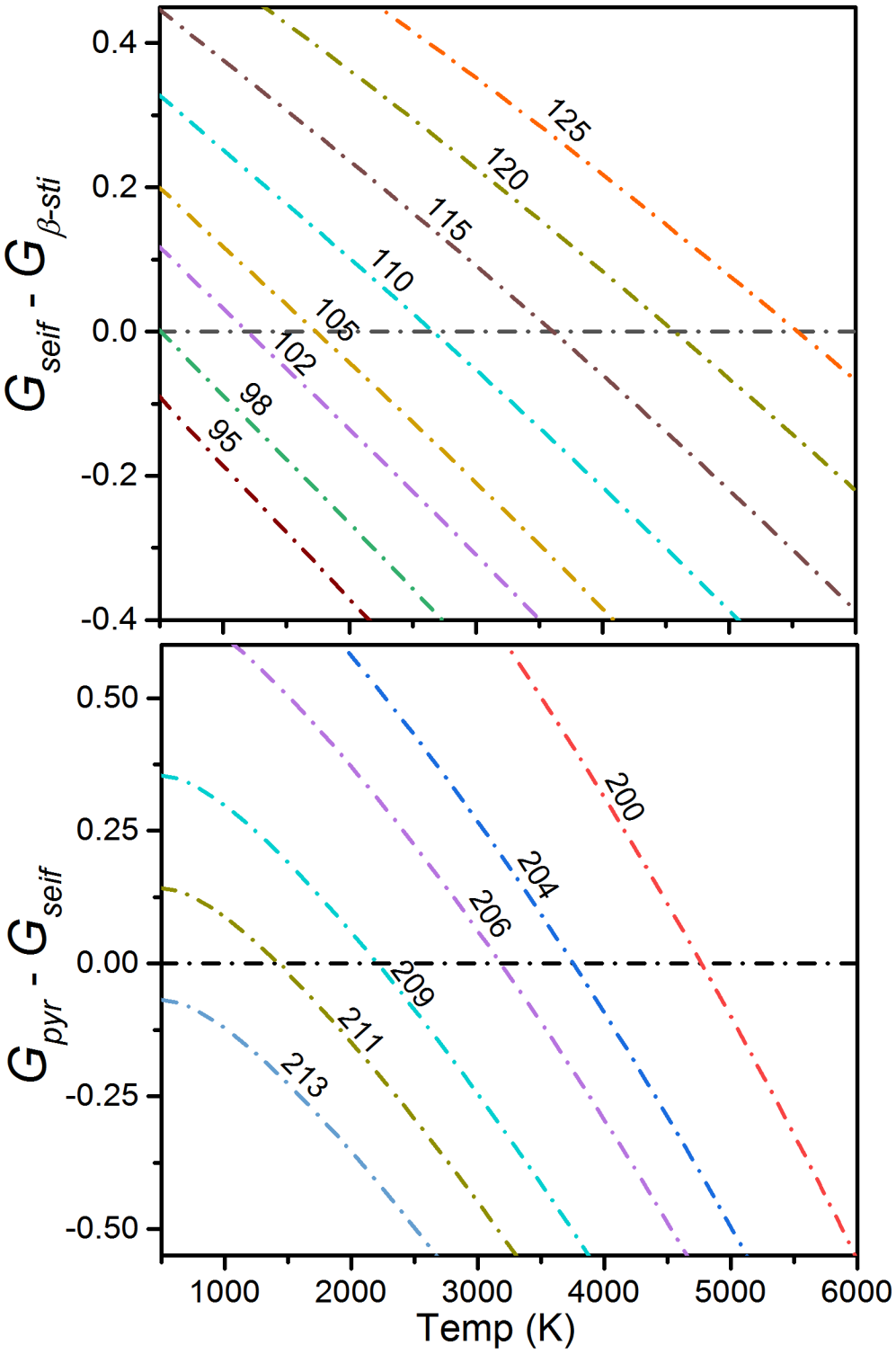

FIGURE 2. Gibbs free energy change upon the phase transition from β-stishovite to seifertite (upper panel) and seifertite to pyrite-type silica (lower) as a function of pressure (contour values in GPa) and temperature, calculated with the GGA functional. The transition pressure increases (positive dp/dT slope) and decreases (negative dp/dT slope) with increasing temperature for the β-stishovite to seifertite and seifertite to pyrite-type phase boundaries, respectively.

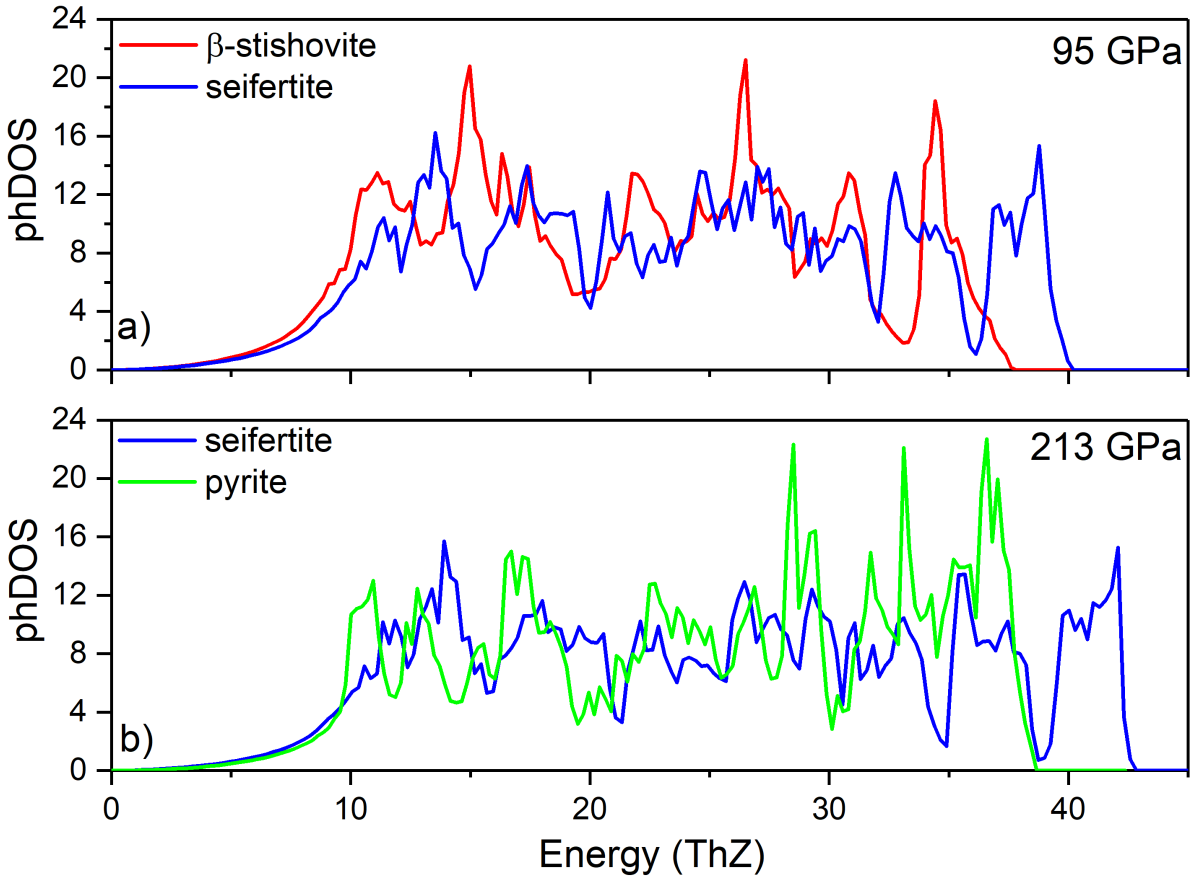

FIGURE 3. Calculated total phonon density of states of three SiO_2 phases from *ab-initio* lattice dynamics. The phDOS is scaled to 3N (N = no. of atoms).

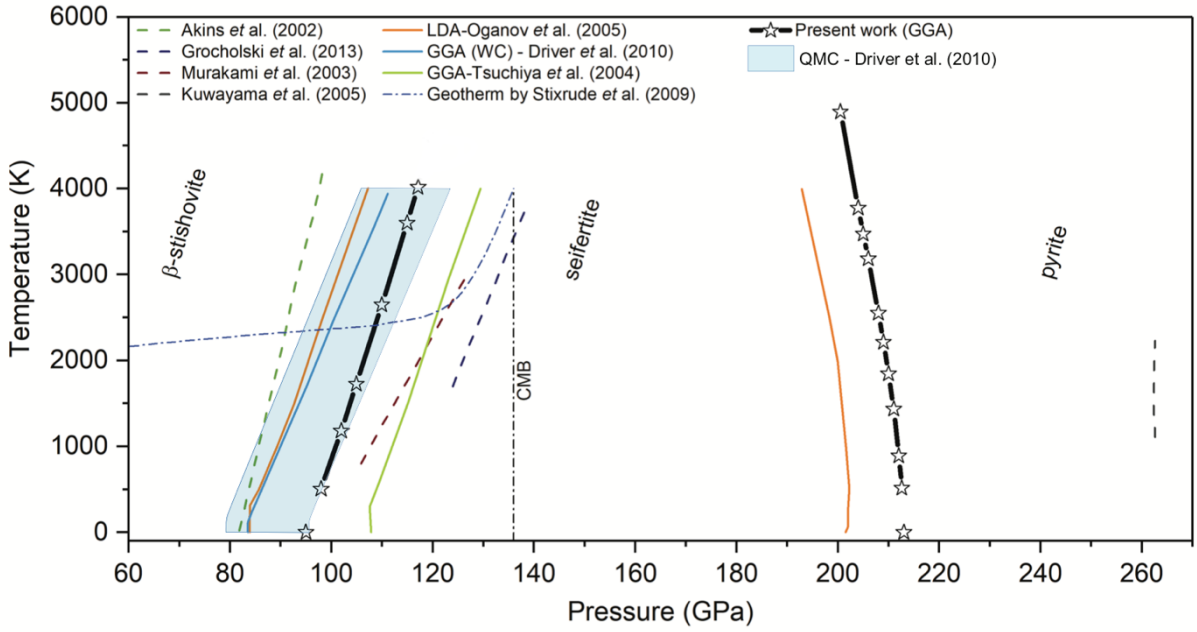

FIGURE 4. Phase boundaries for the β-stishovite to seifertite and seifertite to pyrite-structured silica. The present results are displayed together with previous results (dashed and solid lines represent experimental and theoretical results, respectively). Static transition pressures are without zero point energy correction. The seifertite-forming transition of Stixrude and Lithgow-Bertelloni (2011) is fixed to the Murakami et al. (2003) transition. Experiments on compositions with 10 mol% Al_2O_3 form the lower bracket for β-stishovite stability in the Grocholski et al. (2013) study.Within the adiabatic range, the geotherm of Stixrude et al. is only about 5 K above the Brown and Shankland (1981) geotherm at pressures above 80 GPa.

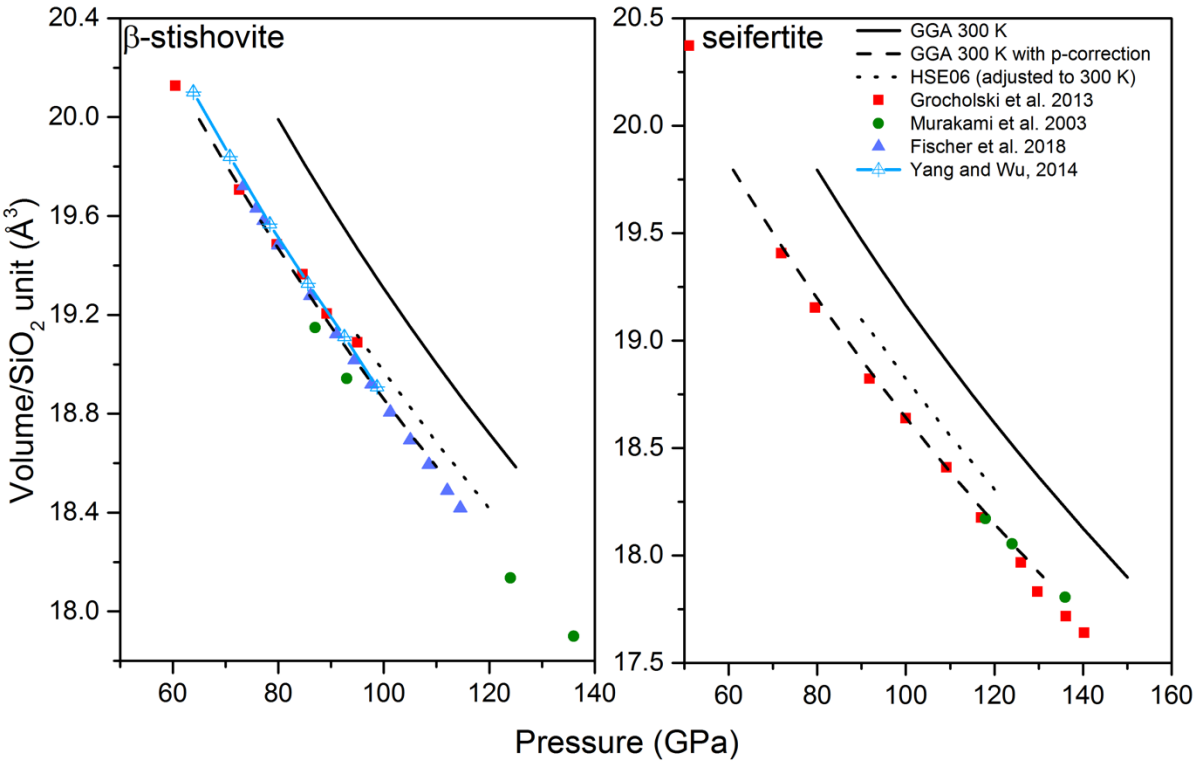

FIGURE 5. Equations of state for β-stishovite and seifertite. The HSE06-based EoS (adjusted to 300 K by adding the GGA-derived volume increase from 0 to 300 K) is similar to the 300 K experimental data of Grocholski et al. (2013), Murakami et al. (2003) and Fischer et al. (2018). The LDA results of Yang and Wu (2014) coincides with the experimental data and the present GGA-based pV-curve has the same functional form as the experimental EoS. To obtain optimal density estimates in Fig. 6, the GGA-curves were adjusted downwards by 15 and 19 GPa for β-stishovite and seifertite, respectively.

Comment to the phase transitions in Fig. 4: Because the GGA-volume of each phase is about 2% larger that the experimentally based volumes in Fig. 5, this difference will be *roughly* cancelled out in $\Delta V = V_{seif} - V_{\beta\text{-stish}}$ and the Clapeyron relation, $dp/dT = \Delta S/\Delta V$. Because the static limit GGA and HSE06 pressures for the β-stishovite to seifertite and seifertite to pyrite-type phase transitions differ by only 1.0 and 0.8 %, respectively (Fig. 1), we have not employed any volume or pressure correction to the phase transitions in Fig. 4.

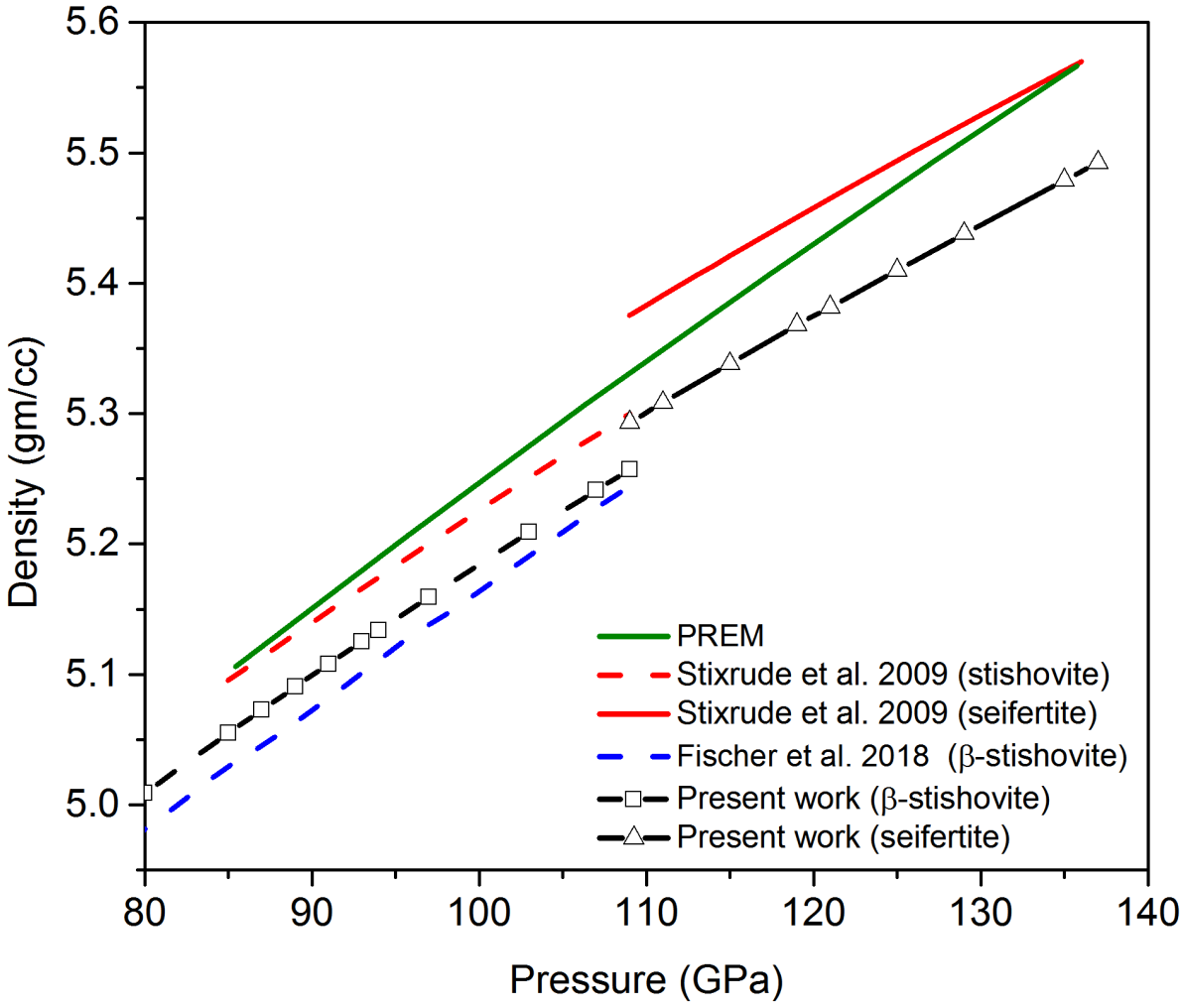

Figure 6. Density of silica phases calculated by the BurnMan code (Cottaar et al., 2014) along the default adiabat of Brown and Shankland (1981), extended to 136 GPa and about 2450 K. Our predicted density for seifertite is 1.5 % lower than the HeFESTo-value of Stixrude and Lithgow-Bertelloni (2011). The density curves are truncated at the seifertite-forming boundary (at 109 GPa and 2400 K). Note that the Stixrude and Lithgow-Bertelloni (2011) density curve below the seifertite stability range is for stishovite, rather than for β-stishovite.

High pressure silica phase transitions: Implications for deep mantle dynamics and silica crystallization in the protocore

Pratik Kr. Das[1], Chris E. Mohn[1], John P. Brodholt[1,2], Reidar G. Trønnes[1,3]
[1]Centre for Earth Evolution and Dynamics, University of Oslo
[2]Department of Earth Sciences, University College London
[3]Natural History Museum, University of Oslo

Supplementary material: Crystal structures of β-stishovite, seifertite and pyrite-structured silica. The common structural units are SiO_6-octahedra, which are variably linked and oriented. The crystallographic axes are uniformly color-coded: a, red; b, green; c, blue.

β-stishovite

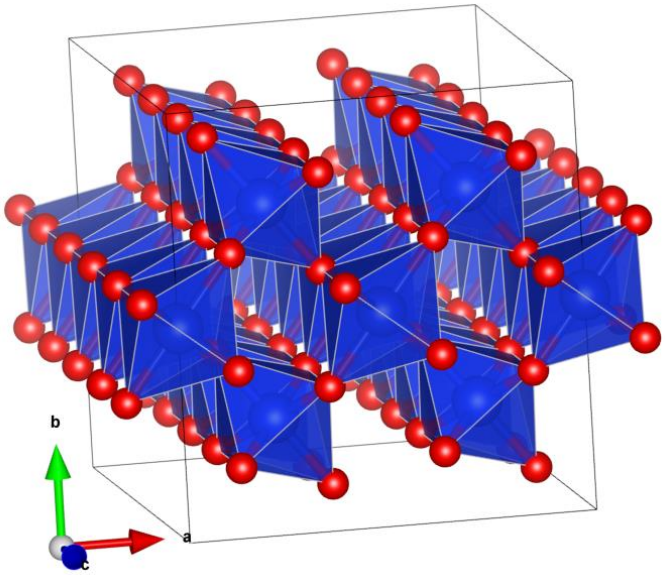

Fig. S1: Edge-sharing SiO_6-octahedra along the c-axis form ac-layers normal to the b-axis. Two alternating ac-layers, made of oppositely tilted SiO_6-octahedra, are connected by corner-sharing octahedra.

Seifertite

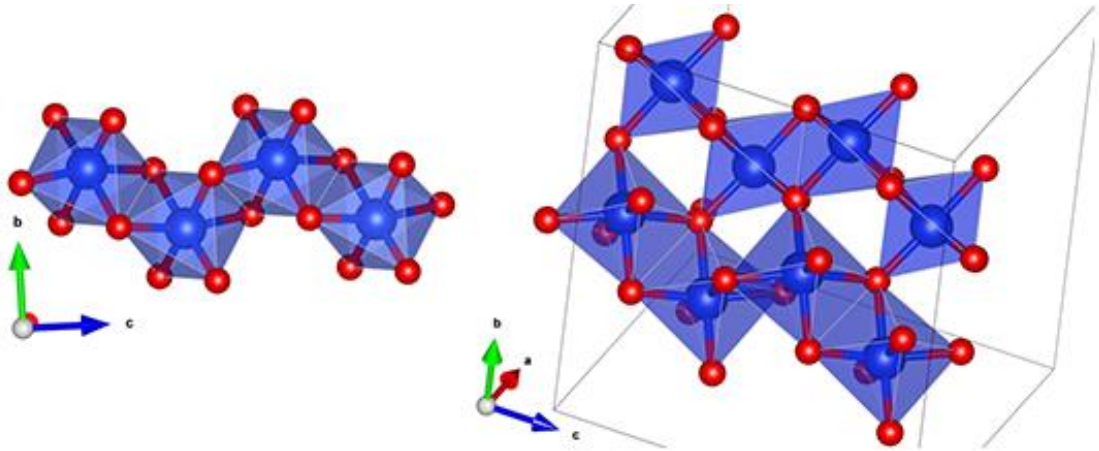

Fig. S2: Edge-sharing SiO_6-octahedra form octahedral layers parallel to the bc-plane. Each of the edge-sharing octahedra along the c-axis is rotated relative to its neighbors, forming a zig-zag pattern. The bc-layers are connected to each other along the a-axis by corner-linked octahedra.

Pyrite-structures silica

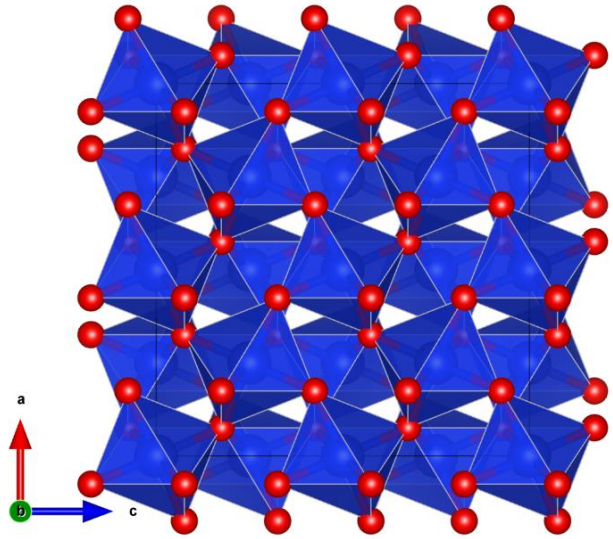

Fig. S3: All of the SiO_6-octahedra are corner-linked in the pyrite-type silica phase. Each corner of the SiO_6-octahedra is connected to another two octahedra. This close-packing may be the reason for higher entropy reflected by phonon-DOS